



Polyol method and surface functionalization of silver nanowires using bovine serum albumin for surface-enhanced Raman scattering application

Khoa Tien CAO¹, Khoi Khac TRAN², and Hue Thi DO^{1,*}

¹ Faculty of Physics, Thai Nguyen University of Education, No. 20, Luong Ngoc Quyen Street, Quang Trung Ward, Thai Nguyen City, 25000, Viet Nam

² Faculty of Fundamental Science, Phenikaa University, Nguyen Van Trac Street, Yen Nghia Ward, Ha Dong District, Hanoi City, Ha Dong, 100000, Vietnam

*Corresponding author e-mail: huedt@tnue.edu.vn

Received date:

3 May 2023

Revised date

4 July 2023

Accepted date:

8 July 2023

Keywords:

Polyol method;
Functionalization;
Silver nanowires (AgNWs);
AgNW@BSA;
Surface-enhanced Raman scattering (SERS).

Abstract

Silver nanowires (AgNWs) with diverse applications are attracting the attention of many researchers around the world. In this study, we applied the polyol method to synthesize AgNWs based on Polyvinylpyrrolidone (PVP) average molecular weight of 360,000, ethylene glycol (EG), and AgNO₃ precursor with a fresh AgCl preparation. To synthesize this material we first investigate optimal parameters through the influence of reaction temperature, time of creating AgNWs using plasmon absorption spectroscopy, and scanning electron microscope (SEM) images. The obtained AgNWs are high efficiency, large aspect ratio, and good dispersion in the solution. This sample continues to be conducted to surface functionalization by bovine serum albumin (BSA) molecules to develop AgNW@BSA complexes. We apply UV-Vis absorption spectroscopy to evaluate the optical properties of these complexes. Besides, we conduct research on the application of this material on surface-enhanced Raman scattering (SERS). The results show that the optical properties of these complexes obtained from UV-Vis absorption spectroscopy are comparable with the numerical modeling. In addition, AgNWs can be used to study the effective surface-enhanced Raman scattering (SERS) to detect methylene blue (MB) molecules at low concentrations as 10⁻¹² M.

1. Introduction

Silver nanostructures are common materials that have been applied in many fields. AgNWs display various optical properties for their different shapes or sizes leading to diverse applications. For example, the AgNWs are a potential material to replace materials commonly used for optoelectronic devices because of their flexibility and characteristic electrical properties [1]. The AgNWs are the main elements in the electrode in flexibility which is an extremely important part of flexible electronic devices (e.g., flexible organic light-emitting diodes (OLEDs), touch screens, and solar cells) [2-4]. The AgNWs have been used as an alternative material to Indium tin oxide (ITO) in sensors, energy devices, and electronics [5-7]. Besides, AgNWs are also a good choice for enhancing surface Raman signals for detecting organic dyes such as other silver nanostructures [8-13].

Synthesizing the AgNWs have been considered in various methods. For example, proposed the electrochemical method to obtain the AgNWs with DNA as a template [14]. AgNWs were synthesized by sonoelectrochemical reactions in the presence of AgNO₃ solution and ethylenediamine tetraacetic acid (EDTA) under the N₂ atmosphere. The results obtained AgNWs with a diameter of 40 nm and a length of up to over 6 μm [15]. T. W. Kim *et al.*, (2017) performed the irradiation method to achieve the AgNWs, where the shapes of the AgNWs were affected by melting during the thermal degradation process [16].

D. B. Barkey *et al.* (2019), Li Wang *et al.* (2018), J. J. Huang *et al.* (2015) in their researches considered the polyol method to synthesize AgNWs by a simple and economical synthesis process, many studies have resulted in synthesis processes and the improvement of existing ones [17-19]. To increase the photoelectric efficiency of AgNWs, Niu *et al.* (2018) have synthesized AgNWs with a diameter of about 13 nm, and a length of about 40 m by using the polyol method in the presence of benzoin radicals [20]. To minimize the generation of by-products in the polyol method, the effects of AgNO₃ concentration, PVP concentration, used PVP molar mass, and rate of PVP were investigated [17-19,21-23]. However, the formed AgNWs obtained from the above methods still have dendrites and by-products because of the viscosity of the solvent in the solution [14-16,24]. Among methods to synthesize AgNWs, the polyol method gives the highest synthesis efficiency, controlling a uniformity, aspect ratio, and especially saving time and cost. Most of the studies used the available AgCl, so the synthesis efficiency is not high because there are many by-products. Therefore, this study applies the polyol method by optimizing the synthesis parameters including reaction time, and temperature. We also use the newly synthesized AgCl to catalyze the synthesis of AgNWs. Besides, we investigate the optical properties of AgNWs after surface functionalizing by BSA molecules and evaluate them by comparing these properties to the modeling method. The application of SERS of branched and unbranched meso silver structures [8,10,25],

silver nanorods [11-13] in the detection of toxic organic dye has been studied in many of our previous publications. To complement that research system in this paper the obtained AgNWs are used to investigate the effective surface-enhanced Raman scattering applied in detecting the organic pigment methylene blue (MB).

2. Experimental

2.1 Necessary chemicals

To synthesis of the AgNWs, requires sufficient chemicals. We prepare high-quality chemicals including the Polyvinylpyrrolidone (PVP, (C₆H₉NO)_n, 360,000 MW), the silver nitrate (AgNO₃, 99%), and the Bovine Serum Albumin (≥ 98.0% (GE)) which provided by Sigma Aldrich company. In addition, the Sodium chloride (NaCl, 99.8%), methylene blue (MB), and ethylene glycol (EG, C₂H₆O₂, 99.8%) were supplied by Merck company. Besides, we synthesize the deion water. We used these chemicals directly without any additional process.

2.2 Synthesis of AgNWs

We synthesize the AgNWs using pure AgCl which is obtained from a reaction of AgNO₃ and NaCl. To collect AgCl, we also put 10 mL of 0.5 M AgNO₃ solution into a flask containing 10 mL of 1 M NaCl solution. The mixture is stirred slowly at 800 rpm for approximately one minute, and a white precipitate appeared as fresh AgCl. The AgCl precipitate is extracted from this solution. Obtained AgCl is washed with deionized water and dried under a vacuum at 50°C for 12 h.

We prepare a flat-bottomed three-neck flask where the 1.7 g of PVP 360,000 MW is dispersed in 100 mL of EG. This solution is magnetically stirred at 800 rpm with the temperature values controlled between 130°C and 170°C in steps of 10°C. As the temperature in the flask reaches equilibrium (about 10 min after magnetic stirring), we put the 125 mg of above fresh AgCl into the solution and it immediately turns bright yellow. After five min, we put 0.5 g of solid AgNO₃ into this reaction vessel. The three-necked flasks are always fully sealed by caps and double-sided tape throughout the reaction. In this process, AgNWs are formed. To investigate the formation of AgNWs over time, the 5 mL of solution is rapidly extracted from the reaction vessel at certain times as material for conducting the necessary investigations.

2.3 Functionalization of silver nanowires by BSA (AgNW@BSA)

To develop the AgNW@BSA, we put 30 μL, 50 μL and 60 μL of 0.1 M BSA solution into three flasks containing 10 mL of AgNWs solution, respectively. These mixtures are reacted at a temperature of 150°C. After that, they are stirred for 1 h at room temperature (25°C to 30°C). After 1 h, we conduct centrifuged these mixtures three times at 3000 rpm for 15 min each time to remove excess BSA. The precipitate is redispersed by double-distilled water to approach the initial volume (10 mL). Once the solutions have been collected, we use them to investigate their optical properties using UV-Vis absorption spectroscopy.

2.4 Investigate the surface-enhanced Raman scattering effect of AgNWs

We examine the SERs effect of AgNWs via Raman scattering spectroscopy. The Raman spectra are collected utilizing a Raman spectrometer (Raman Horiba XploRa plus Raman microprobe) made in France. This device consists of a laser beam with an excitation wavelength of 532.0 nm, a diameter of 4.0 mm, a laser power of 3.2 mW, and a reception time of 8.0 s. Therefore, it can provide a reasonable output. To investigate the SERs effect of AgNWs, we first clean and condense the collected AgNWs. Secondly, we spread the condensed AgNWs onto glass substrates to form small dots one mm in diameter. This material serves as SERs substrates to detect MB pigment. Finally, the 10 μL MB dye of different concentrations from 10⁻¹³ M to 10⁻⁴ M is slowly added to the SERs substrates also keeping the SERs substrate diameter constant to serve as Raman probes.

3. Results and discussion

The optical properties of AgNWs are due to the interaction of the electromagnetic field of the incident light with the electrons on the surface of the nanowire, known as the surface plasmon resonance effect. The electromagnetic field distribution of the incident light strongly depends on the shape and structure of the metal nanoparticles, therefore, the optical properties of the AgNWs depend on their aspect ratio. To investigate the influence of temperature on the growth and formation of AgNWs, we perform the experiments at the same parameters and change only the temperature. The reaction temperature is adjusted from 130°C to 170°C. Figure 1 shows the results of the influence of temperature on the formation of AgNWs. At the temperature of 130°C, the absorption spectra do not appear as plasmon resonance peaks ranging from 300 nm to 1000 nm. This demonstrates that the temperature of 130°C has no impact on the formation of silver nanoparticles. For the reaction at the temperature of 140°C, the absorption spectrum of the solution resembles that of spherical silver nanoparticles, exhibiting a surface plasmon resonance peak at 400 nm to 500 nm for the initial 20 min. However, after 25 min of reaction, the absorption spectrum of the solution emerges four plasmon resonance peaks. One of them is 350 nm, and the remaining three peaks tend to shift towards the long wave as the reaction time increases. The appearance of resonance peaks at 350 nm and around 400 nm implies the contribution of the silver nanorods. While, the appearance of two resonance peaks at the long wave distributes the contribution of electrons from other structural silver nanoparticles. This indicates that silver nanoparticles with various shapes are manifested in the solution at a temperature of 140°C. For the reaction temperature ranging from 150°C to 170°C, the absorption spectra of the obtained solution present a similar form. The contribution of surface plasmon resonance peaks as well as the peak position depends on the horizontal size and length of AgNWs [26-28]. Initially, spherical nanoparticles are formed in the solution, displaying a resonance peak at 408 nm. Subsequently, over time, these nanoparticles underwent growth and transformed into AgNWs, characterized by two resonance peaks located at 350 nm and 377 nm. The resemblance of the spectra indicates the exclusive formation of AgNWs in the solution. In addition, the rate of AgNWs formation is directly proportional to the temperature, with higher

temperatures resulting in faster formation. At a temperature of 140°C, beside the silver nanorods (AgNRs) the solution consists many of silver nanocubes as shown in Figure 1(b). The aspect ratio of these AgNRs is about 20, moreover, there are AgNRs with a very large aspect ratio (Figure 2(a)). When the temperature increases from 150°C upward, only AgNRs appear relatively uniform with a high aspect ratio.

When the aspect ratio is above 1000, the AgNRs are considered as one-dimensional structural materials, also known as silver nanowires (AgNWs). As the temperature increases, the obtained AgNWs exhibit a longer aspect ratio. Figure 2 shows the SEM images of silver nanoparticles synthesized at different temperatures. The inserted figures are the particle solutions after the end of the reaction.

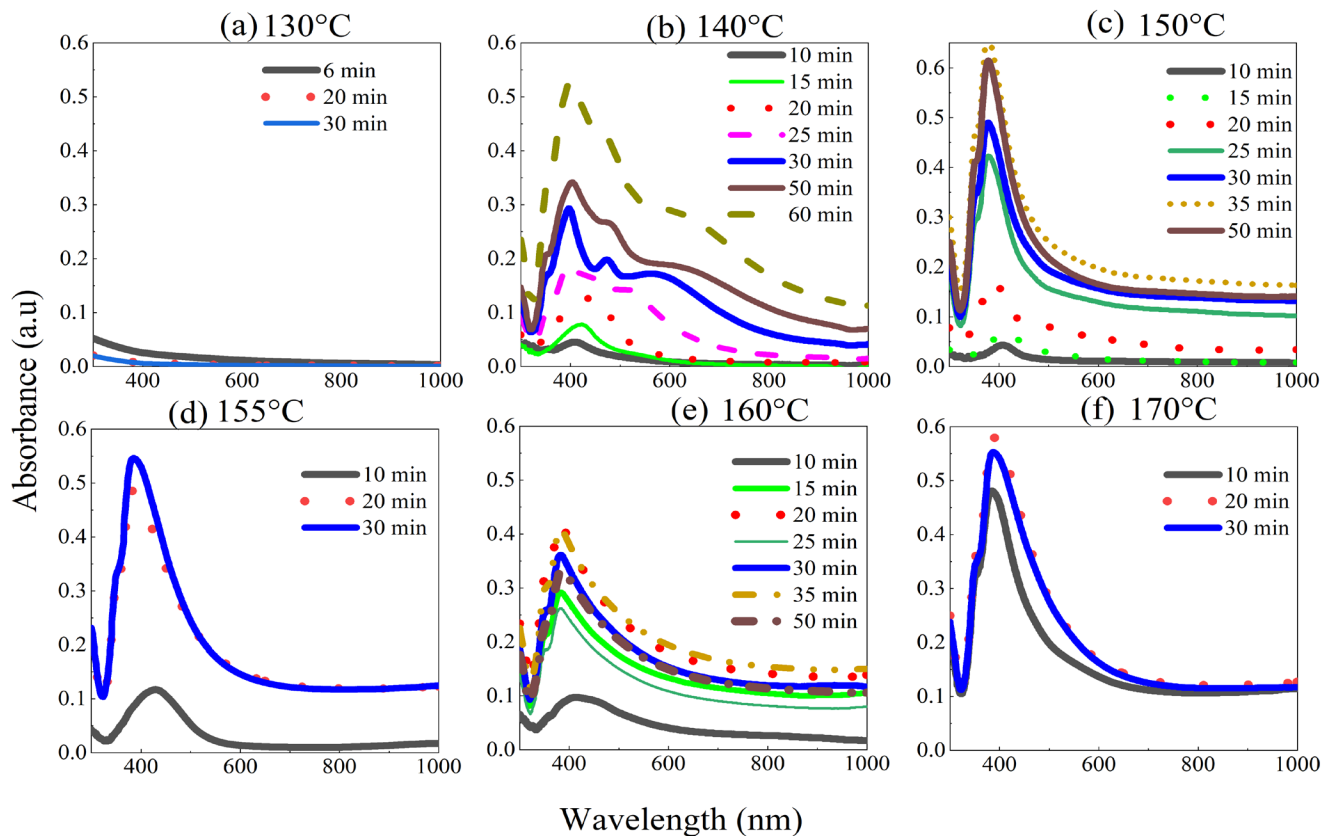


Figure 1. UV-Vis absorption spectra over time of the synthesized solutions at different temperatures: (a) 130°C, (b) 140°C, (c) 150°C, (d) 155°C, (e) 160°C, and (f) 170°C.

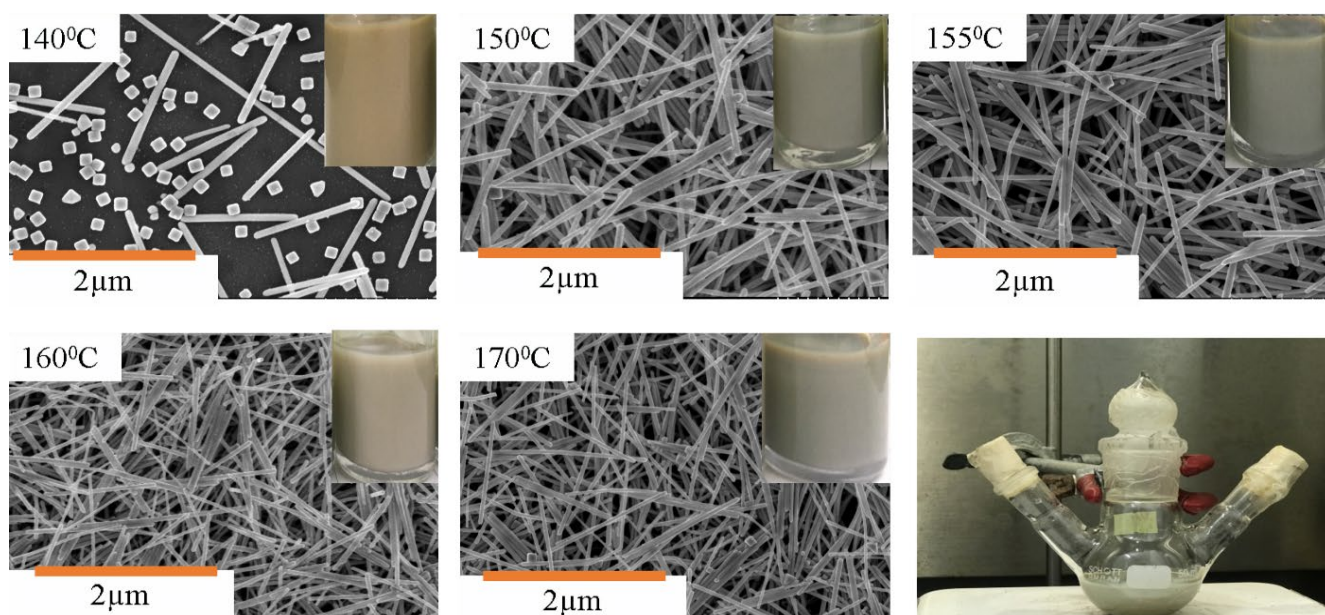


Figure 2. SEM images of silver nanoparticles synthesized at different temperatures (140°C to 170°C) and a photo of a sample during the reaction. The images have the same 2 μm scale.

When the reaction time is increased, various resonance modes appear at different temperature thresholds, indicating a change in the structure of silver nanoparticles in the solution. Furthermore, at different reaction temperatures, the plasmon resonance peak corresponding to the highest absorption peak shifts towards shorter wavelengths over time. While, at the end of the reaction, the wavelength corresponding to the resonance peak remains relatively stable. In addition, for the normalized absorption spectra, the absorbance at 320 nm close to zero is a signal of a completed reaction. Moreover, at a higher temperature, the rate of reaction is faster. For example, the reaction completes after 60 min at the temperature of 140°C, while the significantly shorter times of 25 min, 15 min, and 10 min are reaction times of solution at 150°C, 160°C, and 170°C, respectively. Figure 3(a-d) presents the normalized absorption spectra of the solutions over reaction time for various temperatures (i.e., 140°C, 150°C, 160°C, and 170°C). During the reaction, the normalized absorption peak shift towards the short wave with increasing temperature from 150°C to 170°C. However, Figure 3(e) shows that the normalized absorption peak shifts slightly toward the long wave when the temperature changed from 150°C to 170°C at the end of the reaction. Figure 3(f) indicates the kinetic growth of silver nanostructures in the solution. The absorbance dependence at 350 nm of the spectra is normalized to the 377 nm absorption peak with respect to the reaction time. The gradual increase in size of AgNWs is observed through their kinetics of slow growth. During

the initial period of the reaction (i.e., 25 min for the synthetic sample at 150°C, and 15 min for the synthetic sample at 160°C) spherical silver nanoparticles underwent slow elongation to form AgNRs, which were subsequently rapidly converted to AgNWs via a kinetic process. The rate of transition from spherical to AgNWs increases with higher temperature.

Figure 4(a-d) show the SEM images of samples synthesized at 150°C at different reaction times (i.e., 10 min, 15 min, 30 min, and 60 min) with the same scale of 2 μm . At different reaction times, the AgNPs display different shapes and sizes, because of the growth kinetics of the AgNPs in solution over time. At the first initial 15 min of the reaction, the AgNPs present various morphologies including AgNRs and Ag nanospheres. After 30 min of reaction, AgNWs with a diameter of 20 nm are formed. Until 60 min of reaction, these AgNWs are relatively uniform in shape and size, longer in length and smaller 20 nm in diameter. After 60 min, the particles exhibit negligible growth. The rate of growth of AgNWs from 30 min until the termination of the reaction is comparatively slower than that observed in the initial stages of the reaction. Figure 4(e) shows the change in color of the solution at different reaction times. During the initial 15 min interval, a distinct alteration in the color of the solution is perceptible, while only slight color changes are apparent during the succeeding time intervals. Thus, there is a consistency between the results obtained from the absorption spectra to the SEM images of the particles.

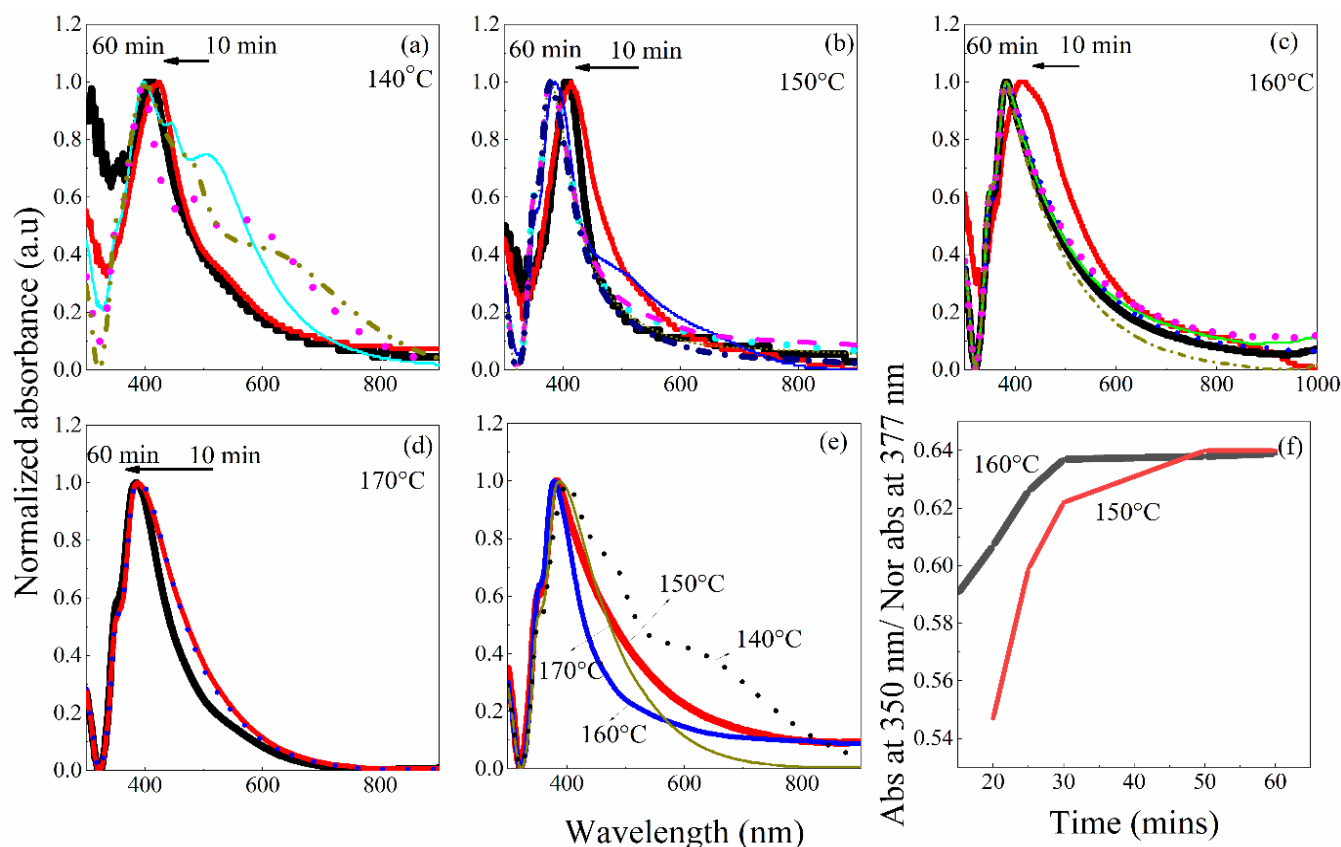


Figure 3 Normalized absorption spectra of solutions over reaction time at different temperatures 140°C (a), 150°C (b), 160°C (c), 170°C (d), the normalized absorption spectra of the solutions at different temperatures at the end of the reaction (e), and the dependence of the ratio between the absorbance at 350 nm and the normalized absorbance at 377 nm wave over time (f).

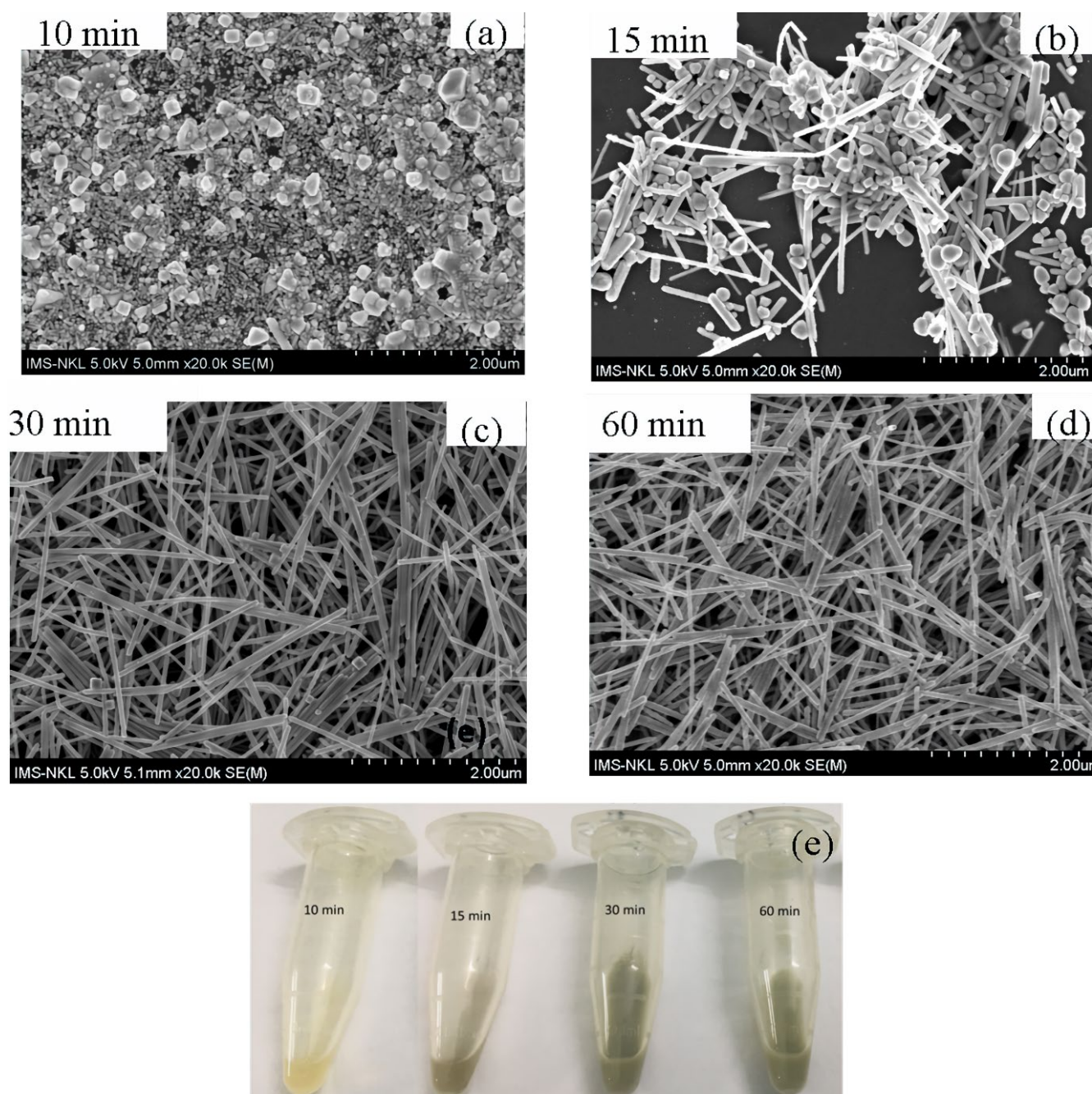


Figure 4. SEM images of samples synthesized at 150°C with different reaction times: (a) 10 min, (b) 15 min, (c) 30 min, and (d) 60 min, and (e) solution samples obtained from different reaction times: 10 min, 15 min, 30 min, and 60 min.

The formation and growth mechanism of AgNWs has been explained depending on the synthesis methods [29-32]. In the polyol method, AgNWs are formed by reducing Ag^+ ions to Ag^0 atoms in the presence of reducing agents and nanowire growth profiling agents such as PVP and Cl^- ions through surface energy interactions and seed development mechanisms [32,33]. Figure 5 explains the diagram for the kinetic mechanism of the formation and growth of AgNPs in solution. Firstly, Ag atoms are synthesized via the reduction of Ag^+ ions of AgNO_3 by EG at elevated temperatures in the presence of oxygen gas. Nevertheless, the reduction reaction that forms Ag atoms and produces nitric acid HNO_3 could decompose Ag atoms into Ag^+ ions in solution through the reverse process [34] as shown in Figure 5. Ag^+ ions within AgCl also attribute to the formation and

growth of AgNWs, the Ag atoms always tend to form spherical nanoparticles according to the principle of energy minimum. Secondly, depending on the temperature of the reaction, the dissociation constant of AgCl is different, as a result the particles will grow in various directions and form different structures. For example, when the temperature is below 140°C the dissociation constant of AgCl is low (1×10^{-9}), leading to the reaction of $\text{AgCl} \leftrightarrow \text{Ag}^+ + \text{Cl}^-$ (reaction 1) prior a direction from left to the right. The Cl^- ions in the solution bind preferentially to Ag (100), resulting in the AgNPs growing into Ag nanocube crystals. The role of Cl^- ions in the formation of Ag nanocubes has been clearly demonstrated in some previous research [35,36]. Simultaneously, under these conditions of the reaction, a small number of AgNRs are formed by the reduction of Ag^+ ions of EG.

Conversely, when the temperature surpasses 150°C, reaction (1) predominantly proceeds in the reverse direction, thereby increasing the concentration of AgCl within the solution. The rate of displacement of the reaction increases proportionally with the temperature, resulting in an elevation in AgCl concentration. This makes the growth rate from spherical silver nanocrystals to AgNRs and AgNWs even faster. As a result, the AgNWs can be uniformly synthesized within less than 10 min at a high temperature of 170°C. This is followed by anisotropic growth of AgNWs to form AgNWs in the solution. The Cl⁻ ion plays an important role in this process. In addition to providing electrostatic stability when nuclei are formed, Cl⁻ ions also contribute to reducing the concentration of Ag⁺ ions, keeping the growth of nuclei in solution controlled. Furthermore, the crystal planes (100) in the five twinned structure are larger than the crystal planes (111). The (100) plane tends to absorb more PVP than the (111) plane. As a result, the crystal plane (100) is covered with PVP, while the crystal plane (111) has only a thin layer of PVP that allows Ag⁺ to easily diffuse to the (111) plane, resulting in significant one-dimensional anisotropic growth on the (111) face forms AgNWs [35,36].

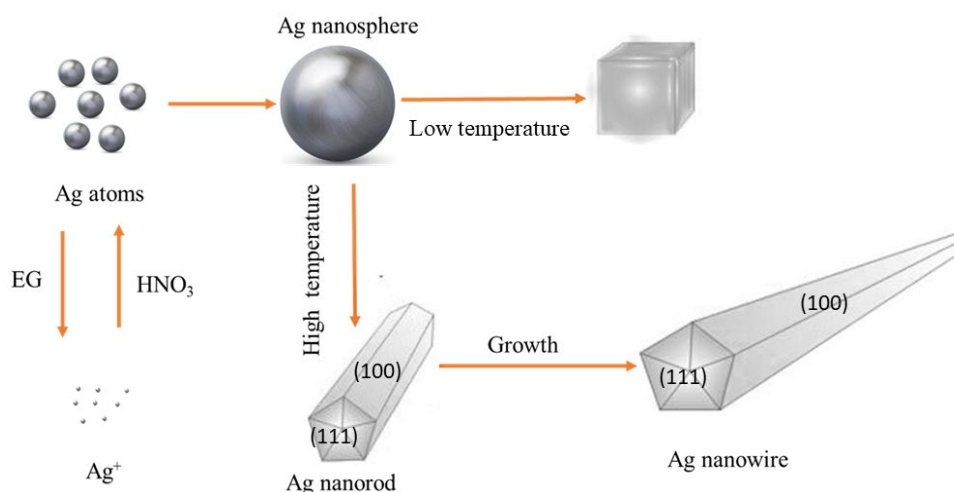


Figure 5. Mechanism of growth and formation of AgNWs.

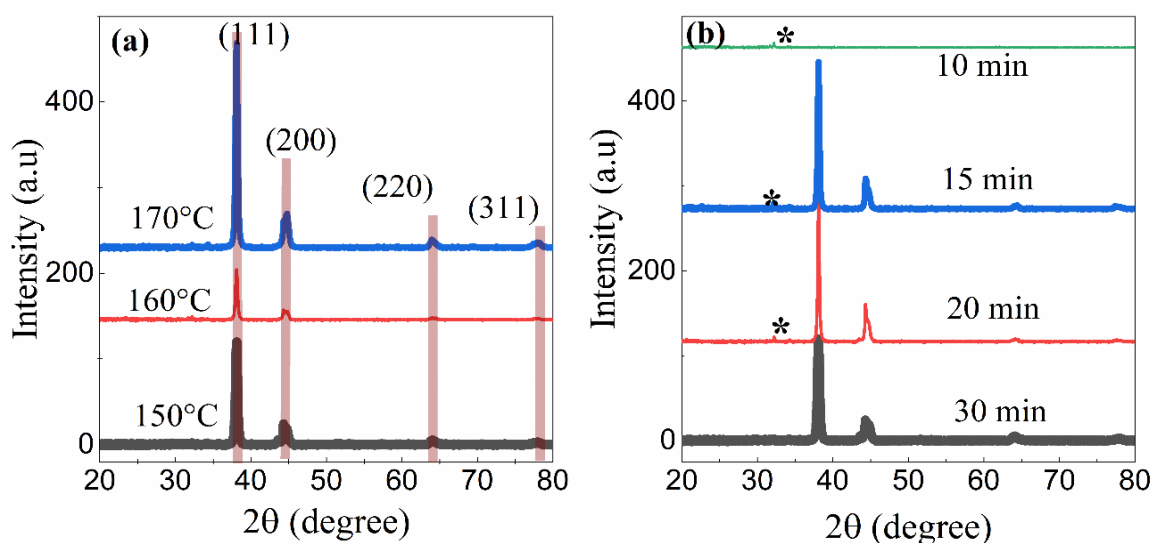


Figure 6. XRD spectra of AgNWs obtained when synthesized at 150°C, 160°C, 170°C (a), and XRD spectra of AgNWs obtained at different reaction times at 150°C (b).

The BSA molecules attach to AgNWs through Van der Waals interactions, forming a protein layer on the AgNWs surface. We observe the conjugation between the BSA protein and AgNWs. We selected AgNWs synthesized at 150°C with a diameter of 20 nm to develop AgNWs@BSA. We investigate the optical properties of the AgNWs before and after the binding of BSA molecules through absorption spectra and normalized absorption spectra of them. The absorption spectra are obtained after removing the unbound BSA molecules in solutions. Figures 7(a-b) illustrate the absorption spectra and normalized absorption spectra of AgNWs as well as AgNWs@BSA. We considered three AgNWs@BSAs (i.e., AgNWs@BSA1, AgNWs@BSA2, and AgNWs@BSA3) with protein layers of varying thicknesses. There are two peaks observed for the absorption spectra of AgNWs @BSAs. The first peak appears at the resonant wavelength 415 nm for three samples of AgNWs @BSAs, and the remaining one has the longer wavelength (i.e., 594 nm, 635 nm, and 654 nm corresponding to AgNWs@BSA1, AgNWs@BSA2, and AgNWs@BSA3, respectively). The difference in spectra before and after binding BSA implies the effectiveness of binding BSA molecules to AgNWs. Before binding to BSA, the absorption spectrum of the AgNW exhibited a distinct resonance peak at 377 nm, accompanied by a low-intensity absorption shoulder at 350 nm. The peak at 377 nm mostly is caused by the oscillation of electrons in the horizontal direction of the AgNWs, the absorption shoulder at 350 nm is the characteristic resonance peak for the bonding interaction of AgNWs in solution. Whereas, the first resonance peak of the absorption spectrum of AgNWs@BSAs at 415 nm which is attributed as a mode corresponding to the transverse vibrational plasmon resonance mode of the electrons in the AgNW shift towards longwave approximately 38 nm compare to the same mode in uncoated AgNWs. This phenomenon is explained as follows: The electromagnetic field propagates to the AgNWs surface, to interact with the BSA molecules in the shell, also decreasing the interaction energy of the electromagnetic field with the electrons on the AgNW surface. The spectrum curves show that the thickness of BSA layers on the AgNWs surface has a significant influence on the optical properties. As the thickness of the BSA shell increases, the low-energy resonance peak shifts towards the longer wavelengths.

Line 1: AgNW@BSA 1 Line 2: AgNW@BSA2 Line 3: AgNW@BSA 3 Line 4: AgNW

The appearance of a second resonance peaks on the long wave in the resonance spectrum of AgNWs@BSAs are not due to the longitudinally oscillating electrons of the wire contributed by lengths up to 2 μm (i.e., aspect ratio above 200). In addition, the longitudinal plasmon resonance peaks of the AgNWs locate in the infrared region. These peaks are not presentative for the BSA, because there is no optical peak of BSA located in the visible light region [37]. Therefore, the appearance of the second resonance peaks are caused by the association of AgNWs@ BSA. Figure 7(c) shows the dependence of the bonding resonance wavelengths on the BSA fill factor of the AgNWs. The fill coefficients of BSA on AgNWs are 0.3, 0.5, and 0.6 corresponding to the low-energy plasmon second resonance peaks at wavelengths of 594 nm, 635 nm, and 654 nm for AgNWs@BSA1, AgNWs@BSA2, and AgNWs@BSA3 respectively.

It implies that when shifting to the longwave direction, the binding resonance wavelength is proportional to the increase of the

filling coefficient. Because the adsorption of BSA and the thickness of the BSA shell cause a change in the dielectric function of the medium around the AgNWs. These results are in good agreement with the effective environment approximation of Mie-Gans [38]. Therefore, we can design the optical properties of AgNWs by adjusting the thickness of protein coat for these nanostructures in order to exploit various applications of them.

We investigate the ability of AgNWs to enhance surface Raman scattering for detecting toxic pigments at low concentrations. Figure 8(a) presents the Raman scattering spectrum of the MB (10^{-4} M) dye on the glass substrate. The scattering peak at 1620 cm^{-1} has the highest relative scattering intensity and it is the most characteristic Raman signal of MB. This number is in good agreement with the characteristic scattering peaks of MB presented by Yuxia Fan [39]. The scattering peaks at wave numbers 1620 cm^{-1} , 1401 cm^{-1} , and 450 cm^{-1} , present the bond patterns $\nu(\text{C}-\text{C})$ ring stretches, $\nu(\text{C}-\text{N})$ symmetric and asymmetric stretches, and $\delta(\text{C}-\text{N}-\text{C})$ skeletal deformation mode, respectively [40,41]. The SERs spectra of MB in different concentrations from 10^{-13} M to 10^{-4} M enhanced on a substrate of AgNWs are shown in Figure 8(b). SERs spectra show that the intensity of the Raman scattering peaks of MB at low concentrations are significantly enhanced compared to the original Raman scattering spectrum of MB. At the same time, on the SERs spectra, there are peaks at 230 cm^{-1} and 1724 cm^{-1} which is not present in the scattering spectrum of MB. These peaks are said to be the characteristic peak of Ag - N or Ag - S of the bond between AgNWs and MB [42,43]. The characteristic scattering peak of MB at 1620 cm^{-1} shifts by about 44 cm^{-1} to 1576 cm^{-1} when enhanced by AgNWs. It might be due to the influence of bond formation between AgNWs and MB molecules. As the concentration of MB increases, the interactions between its bonds become more pronounced, causing a shift in the $\nu(\text{C}-\text{C})$ ring bond stretch away from the original MB scattering peak. The level of enhancement in scattering at a particular peak of the spectrum is evaluated through an enhancement factor (EF). The EF of AgNWs is computed by the Equation below [44]:

$$EF = \frac{I_{\text{SERS}}}{I_{\text{NOR}}} \times \frac{C_{\text{NOR}}}{C_{\text{SERS}}} \quad (2)$$

where I_{SERS} is the Raman signal intensity at 1576 cm^{-1} peak in case the MB molecules adsorbed on AgNWs substrate; I_{NOR} is the Raman signal intensity at 1620 cm^{-1} on a glass; C_{NOR} is the concentration of 10^{-4} M initial MB, and C_{SERS} is the concentration of MB when absorbed on the SERs substrate. we calculated the EF of AgNWs for the largest scattering peak of MB (i.e., 1620 cm^{-1}) at the nine concentrations of 10^{-4} M, 10^{-5} M, 10^{-6} M, 10^{-7} M, 10^{-8} M, 10^{-9} M, 10^{-10} M, 10^{-11} M, and 10^{-12} M respectively: 1.493×10^5 , 1.25×10^6 ; 8.37×10^6 , 7.33×10^7 , 5.98×10^8 , 4.50×10^9 , 2.43×10^{10} , 1.13×10^{11} , 0.9×10^{12} . Furthermore, we consider Raman signal intensity at 1576 cm^{-1} (I_{SERS}) as a parameter depending on the concentration of MB. Figure 8(c) presents I_{SERS} corresponding to various concentrations of MB (denoted by C). We also performed linear regression to obtain a relationship between I_{SERS} and C in logarithmic space through Equation (3).

$$\log(I_{\text{SERS}}) = a \times \log(C) + b \quad (3)$$

where a and b are regression coefficients. They are 0.28 and 6.5, respectively. The fit line and its coefficient of determination (R^2) are presented in Figure 8(c). The R^2 value of 0.91 indicates a closed dependence of the scattering intensity at the 1576 cm^{-1} characteristic peak of enhanced MB in the case of the presence of AgNWs in the concentration of MB dye.

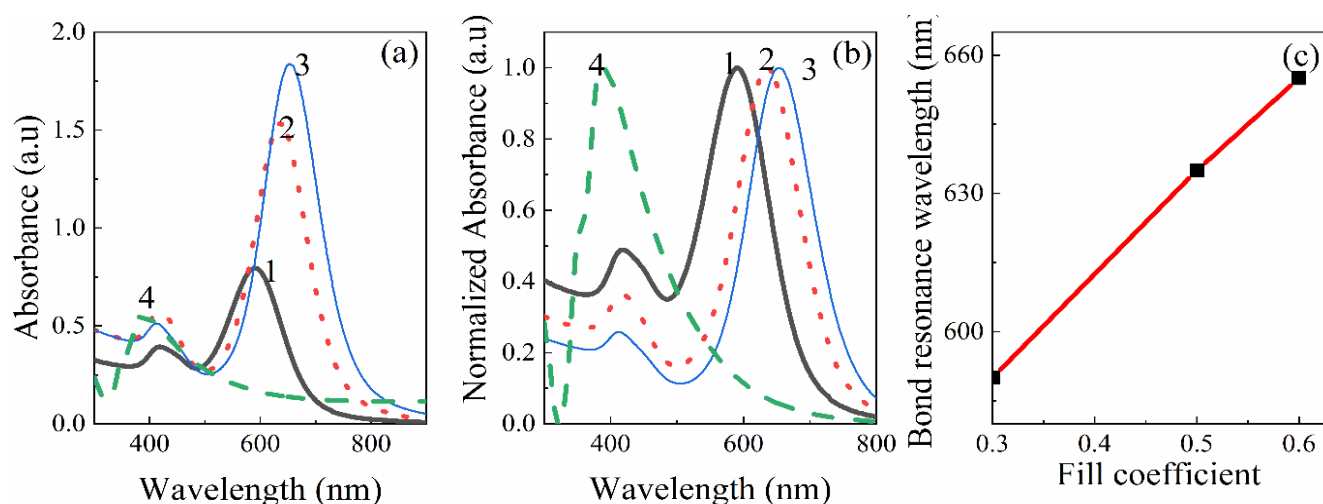


Figure 7. Absorption spectra (a) and normalized absorption spectra (b) of AgNWs s before and after binding to BSA molecules. The dependence of the bond resonance wavelength of AgNWs@BSA on the fill factor (c).

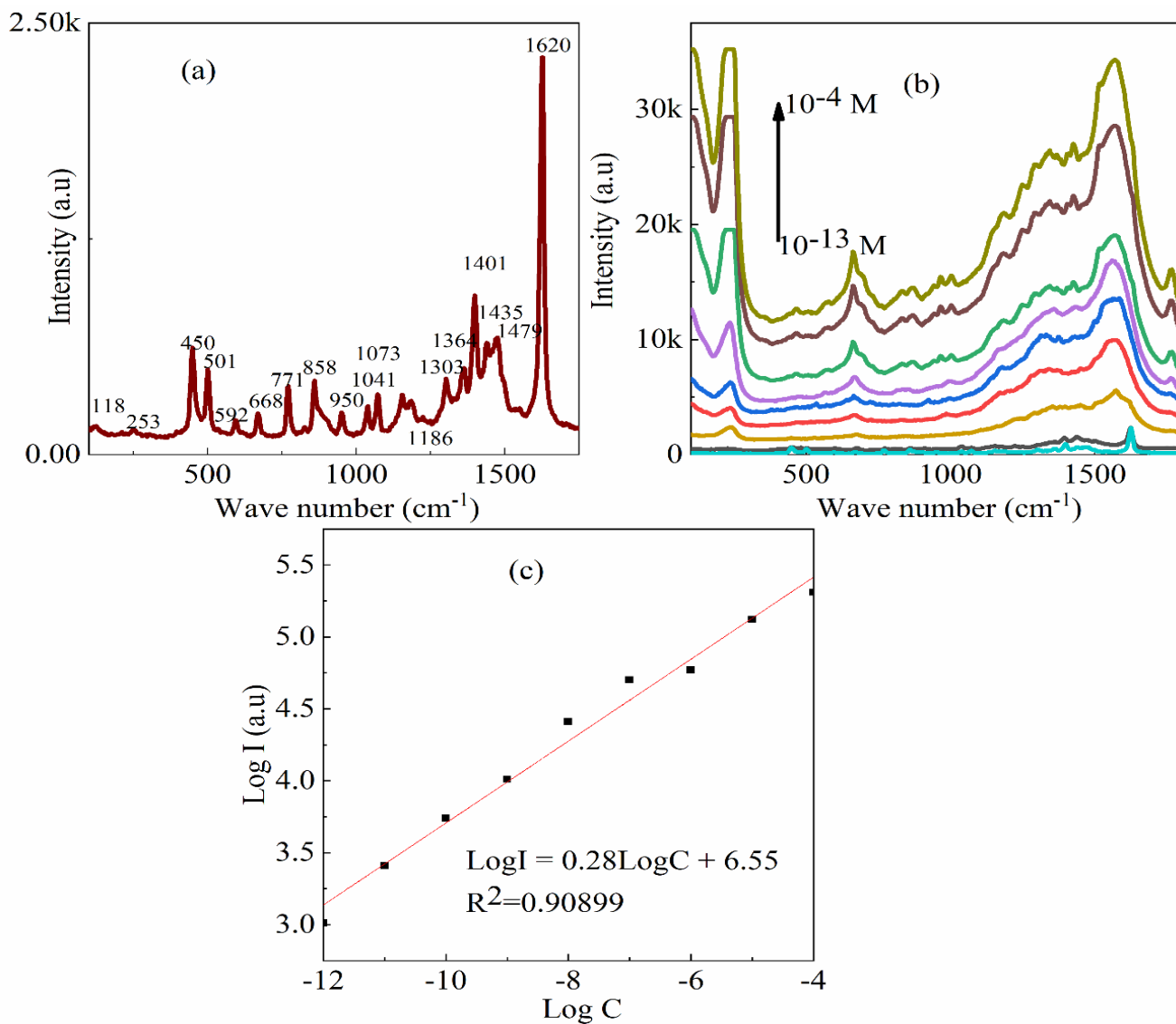


Figure 8. Raman scattering spectrum of MB dye on the glass substrate (a) and SERs spectrum of MB with different concentrations from 10⁻¹³ M to 10⁻⁴ M on AgNWs substrate (b) and dependence the dependence of the scattering intensity (log I) at the characteristic scattering peak of 1620 cm⁻¹ of MB to the concentration of the pigment (log C) (c).

In this study, We synthesize AgNWs considering polyol method using PVP in the presence of ethylene glycol with the new AgCl preparation at various reaction temperatures from 130°C to 170°C. The obtained AgNWs are relatively uniform in shape and size (e.g., a length of over 2 μm and a diameter of smaller than 20 nm) which are reacted at temperatures from 150°C and upwards, and almost no by-products. We evaluated the influence of temperature on the formation and growth of silver nanostructures through UV-Vis absorption spectroscopy, SEM image, and XRD spectrum. The results show that when the reaction temperature is smaller than 140°C, AgNWs appear as a by-product of the reaction to create Ag nanocubes because of the dominance of Cl⁻ ions in the solution. However, with an increase in temperature, the process of AgNWs formation initiates with the generation of spherical silver nanocrystals. These nanocrystals exhibit preferential growth along the (111) facets, transforming into AgNRs, which eventually elongate along an axis to form AgNWs. Furthermore, this process exhibits enhanced kinetics at elevated temperatures. The formation of uniform AgNWs occurred within a duration of less than 10 min at a reaction temperature of 170°C, whereas it took approximately 25 min to achieve the same under a reaction temperature of 150°C.

We develop AgNWs@BSA by binding BSA protein molecules to AgNWs considering three fill coefficients of 0.3, 0.5, and 0.6. We also investigate the optical properties of the AgNWs@BSA by using UV-Vis absorption spectroscopy. The absorption spectra present two characteristic peaks, the higher energy peak corresponds to the horizontal plasmon resonance peak of the AgNWs, and the lower energy resonance peak relates to the alignment of AgNWs @BSA. As the BSA shell becomes thicker, this bonding resonance peak shifts to a longer wavelength. The results on the optical properties of the AgNWs@BSA complex are in good agreement with the theoretical models of the plasmonic properties of the integrated systems. In addition, we use obtained AgNWs for investigating the SERS effect in detecting MB dyes. The results show that the AgNWs can detect MB dye at concentrations as low as 10⁻¹² M with an enhancement factor EF of 0.9 × 10¹².

Acknowledgments

This research is funded by Thai Nguyen University of Education under grant number TNUE-2023-07

Conflict of interest

On behalf of all authors, the corresponding author states that there is no conflict of interest.

References

- [1] S. Raman, and R. S. Arunagirinathan, "Silver nanowires in stretchable resistive strain sensors," *Nanomaterials*, vol. 12, no. 11, 1932, 2022.
- [2] L. Zhang, T. Song, L. Shi, N. Wen, Z. Wu, C. Sun, D. Jiang, and Z. Guo, "Recent progress for silver nanowires conducting film for flexible electronics," *Journal of Nanostructure in Chemistry*, vol. 11, no. 3, pp. 323-341, 2021.
- [3] H. Li, Y. Liu, A. Su, J. Wang, and Y. Duan, "Promising hybrid graphene-silver nanowire composite electrode for flexible organic light-emitting diodes," *Scientific Reports*, vol. 9, no. 1, p. 17998, 2019.
- [4] M. B. Gebeyehu, T. F. Chala, S. Y. Chang, C. M. Wu, and J. Y. Lee, "Synthesis and highly effective purification of silver nanowires to enhance transmittance at low sheet resistance with simple polyol and scalable selective precipitation method," *RSC Advances*, vol. 7, no. 26, pp. 16139-16148, 2017.
- [5] J. Jung, H. Cho, R. Yuksel, D. Kim, H. Lee, J. Kwon, P. Lee, J. Yeo, S. Hong, H. E. Unalan, S. Han, and S. H. Ko, "Stretchable/flexible silver nanowire electrodes for energy device applications," *Nanoscale*, vol. 11, no. 43, pp. 20356-20378, 2019.
- [6] L. Dan, S. Shi, H. J. Chung, and A. Elias, "Porous polydimethylsiloxane-silver nanowire devices for wearable pressure sensors," *ACS Applied Nano Materials*, vol. 2, no. 8, pp. 4869-4878, 2019.
- [7] D. Giasafaki, C. Mitzithra, V. Belessi, T. Filippakopoulou, A. Koutsioukis, V. Georgakilas, G. Charalambopoulou, and T. Steriotis, "Graphene-based composites with silver nanowires for electronic applications," *Nanomaterials*, vol. 12, no. 19, p. 3443, 2022.
- [8] D. T. Hue, N. T. P. Thao, T. K. Khoi, and C. V. Ha, "Multi-shaped silver meso-particles with tunable morphology for surface enhanced Raman scattering," *Optics Communications*, vol. 497, no. 51, p. 127200, 2021.
- [9] T. B. N. Pham, T. T. T. Bui, V. Q. Tran, V. Q. Dang, L. N. Hoang, and C. K. Tran, "Surface-enhanced Raman scattering (SERS) performance on salbutamol detection of colloidal multi-shaped silver nanoparticles," *Applied Nanoscience (Switzerland)*, vol. 10, no. 3, pp. 703-714, 2020.
- [10] C-y. Chin, C-c. Chen, X-a. Chen, H-j. Yen, H-l. Hsien, J-j. Young, and Y-c. Chen, "High sensitivity enhancement of multi-shaped silver-nanoparticle-decorated hydrophilic PVDF-based SERS substrates using solvating pretreatment," *Sensors and Actuators B: Chemical*, vol. 347, no. 15, p. 130614, 2021.
- [11] C. R. Rekha, V. U. Nayar, and K. G. Gopchandran, "Synthesis of highly stable silver nanorods and their application as SERS substrates," *Journal of Science: Advanced Materials and Devices*, vol. 3, no. 2, pp. 196-205, 2018.
- [12] L. Ma, J. Wang, C. Ren, P. Ju, Y. Huang, F. Zhang, F. Zhao, Z. Zhang, and D. Zhang, "Detection of corrosion inhibitor adsorption via a surface-enhanced Raman spectroscopy (SERS) silver nanorods tape sensor," *Sensors and Actuators B: Chemical*, vol. 321, no. 15, p. 128617, 2020.
- [13] D. T. Hue, T. T. Thu Huong, P. T. Thu Ha, T. T. Trang, N. T. Ha Lien, and V. Xuan Hoa, "The dependence of medium refractive index on optical properties of gold nanorods and their SERS application," *AIP Advances*, vol. 11, no. 5, p. 055319, 2021.
- [14] S. Cui, Y. Liu, Z. Yang, and X. Wei, "Construction of silver nanowires on DNA template by an electrochemical technique," *Mater Des*, vol. 28, no. 2, pp. 722-725, 2007.

- [15] J.-J. Zhu, Q.-F. Qiu, H. Wang, J.-R. Zhang, J.-M. Zhu, and Z.-Q. Chen, "Synthesis of silver nanowires by a sonoelectrochemical method." *Communications*, vol.5, no. 4, pp. 242-244, 2002.
- [16] D. C. Choo, and T. W. Kim, "Degradation mechanisms of silver nanowire electrodes under ultraviolet irradiation and heat treatment," *Scientific Reports*, vol. 7, no. 1, Art. 1696, 2017.
- [17] S. Hemmati, M. T. Harris, and D. P. Barkey, "Polyol silver nanowire synthesis and the outlook for a green process," *Journal of Nanomaterials*, vol. 2020. Art. 9341983, 2020.
- [18] S. Fahad, H. Yu, I. Wang, Z. Abdin, M. Haroon, R. S. Ullah, A. Nazir, K. R. Naveed, T. E. M. Ali, and A. Khan, "Recent progress in the synthesis of silver nanowires and their role as conducting materials," *Journal of Materials Science*, vol. 54, no. 2, pp. 997-1035, 2019.
- [19] J. Y. Lin, Y. L. Hsueh, J. J. Huang, and J. R. Wu, "Effect of silver nitrate concentration of silver nanowires synthesized using a polyol method and their application as transparent conductive films," in *Thin Solid Films*, Elsevier B.V., Jun. 2015, pp. 243-247.
- [20] Z. Niu, F. Cui, E. Kuttner, C. Xie, H. Chen, Y. Sun, A. Dehestani, K. Schierle-Arndt, and P. Yang, "Synthesis of silver nanowires with reduced diameters using benzoin-derived radicals to make transparent conductors with high transparency and low haze," *Nano Letters*, vol. 18, no. 8, pp. 5329-5334, 2018.
- [21] J. Bao, J. X. Wang, X. F. Zeng, L. L. Zhang, and J. F. Chen, "Large-Scale synthesis of uniform silver nanowires by high-gravity technology for flexible transparent conductive electrodes," *Industrial and Engineering Chemistry Research*, vol. 58, no. 45, pp. 20630-20638, 2019.
- [22] B. Abel, S. Coskun, M. Mohammed, R. Williams, H. E. Unalan, and K. Aslan, "Metal-enhanced fluorescence from silver nanowires with high aspect ratio on glass slides for biosensing applications," *Journal of Physical Chemistry C*, vol. 119, no. 1, pp. 675-684, 2015.
- [23] H. Sim, C. Kim, S. Bok, M. K. Kim, H. Oh, G-H. lim, S. M. Cho, and B. Lim, "Five-minute synthesis of silver nanowires and their roll-to-roll processing for large-area organic light emitting diodes," *Nanoscale*, vol. 10, no. 25, pp. 12087-12092, 2018.
- [24] W. Liu, K. Wang, Y. Zhou, X. Guan, P. Che, and Y. Han, "Rational synthesis of silver nanowires at an electrode interface by diffusion limitation," *CrystEngComm*, vol. 21, no. 9, pp. 1466-1473, 2019.
- [25] T. B. N. Pham, T. T. T. Bui, V. Q. Tran, V. Q. Dang, L. N. Hoang, and C. K. Tran, "Surface-enhanced Raman scattering (SERS) performance on salbutamol detection of colloidal multi-shaped silver nanoparticles," *Applied Nanoscience (Switzerland)*, vol. 10, no. 3, pp. 703-714, 2020.
- [26] R. D. Abdel-Rahim, A. M. Naguib, O. A. Pharghaly, M. A. Taher, E. S. Yousef, and E. R. shaaban, "Optical properties for flexible and transparent silver nanowires electrodes with different diameters," *Optical Materials*, vol. 117, p. 111123, 2021.
- [27] X. Yang, D. X. Du, and Y. H. Wang, "Length-dependent electro-optical properties of silver nanowires-based transparent conducting films," *Journal of Materials Science: Materials in Electronics*, vol. 30, no. 7, pp. 6838-6845, 2019.
- [28] M. Ćwik, D. Buczyńska, K. Sulowska, E. Roźniecka, S. Mackowski, and J. Niedziółka-Jönsson, "Optical properties of submillimeter silver nanowires synthesized using the hydrothermal method," *Materials*, vol. 12, no. 5, p. 721, 2019.
- [29] P. Zhang, I. Wyman, J. Hu, S. Lin, Z. Zhong, Y. Tu, Z. Huang and Y. Wei, "Silver nanowires: Synthesis technologies, growth mechanism and multifunctional applications," *Materials Science and Engineering B: Solid-State Materials for Advanced Technology*, vol. 223, pp. 1-23, 2017.
- [30] D. Ramirez, and F. Jaramillo, "Facile one-pot synthesis of uniform silver nanoparticles and growth mechanism," *DYNA (Colombia)*, vol. 83, no. 198, pp. 165-170, 2016.
- [31] W. M. Schuette, and W. E. Buhro, "Polyol synthesis of silver nanowires by heterogeneous nucleation; Mechanistic aspects influencing nanowire diameter and length," *Chemistry of Materials*, vol. 26, no. 22, pp. 6410-6417, 2014.
- [32] S. Patil, P. R. Kate, J. B. Deshpande, and A. A. Kulkarni, "Quantitative understanding of nucleation and growth kinetics of silver nanowires," *Chemical Engineering Journal*, vol. 414, p. 128711, 2021.
- [33] M. Parente, M-v. Helvert, R. F. Hamans, R. Verbroekken, R. Sinha, A. Bieberle-Hutter, and A. Baldi, "Simple and fast high-yield synthesis of silver nanowires," *Nano Letters*, vol. 20, no. 8, pp. 5759-5764, 2020.
- [34] K. W. Shah, and T. Xiong, "Multifunctional metallic nanowires in advanced building applications," *Materials*, vol. 12, no. 11, 2019.
- [35] F. Wu, W. Wang, Z. Xu, and F. Li, "Bromide (Br) - Based Synthesis of Ag Nanocubes with High-Yield," *Scientific Reports*, vol. 5, Art. 10772, 2015.
- [36] Z. Chen, T. Balankura, K. A. Fichthorn, and R. M. Rioux, "Revisiting the polyol synthesis of silver nanostructures: role of chloride in nanocube formation," *ACS Nano*, vol. 13, no. 2, pp. 1849-1860, 2019.
- [37] A. Scarangella, M. Soumbo, C. Villeneuve-Faure, A. Mlayah, C. Bonafos, M-C. Monje, C. G. Roques, and K. Makasheva, "Adsorption properties of BSA and DsRed proteins deposited on thin SiO₂ layers: Optically non-absorbing versus absorbing proteins," *Nanotechnology*, vol. 29, no. 11, p. 115101, 2018.
- [38] M. Quinten, "Front Matter," in *Optical Properties of Nanoparticle Systems: Mie and beyond*, Wiley, 2011.
- [39] C. Li, Y. Huang, K. Lai, B. A. Rasco, and Y. Fan, "Analysis of trace methylene blue in fish muscles using ultra-sensitive surface-enhanced Raman spectroscopy," *Food Control*, vol. 65, pp. 99-105, 2016.
- [40] K. Kairyte, A. Kadys, and Z. Luksiene, "Antibacterial and antifungal activity of photoactivated ZnO nanoparticles in suspension," *Journal of Photochemistry and Photobiology B*, vol. 128, pp. 78-84, 2013.
- [41] T. T. H. Pham, X. H. Vu, T. T. Trang, N. X. Ca, N. D. Dien, P. V. Hai, N. T. H. Lien, N. T. Nghia, and T. T. K. Chi, "Enhance Raman scattering for probe methylene blue molecules adsorbed on ZnO microstructures due to charge transfer processes," *Optical Materials*, vol. 120, p. 111460, 2021.
- [42] J. Tang, H. Sun, X. Li, F. Liang, and T. Jiang, "Chemical-etched silver nanowires with tunable rough shape for surface

enhanced Raman scattering,” *Colloids and Surfaces A: Physico-chemical and Engineering Aspects*, vol. 630, 2021.

- [43] G. Lu, H. Yuan, L. Su, B. Kenens, Y. Fujita, M. Chamtour, M. Pszona, E. Fron, J. Waluk, J. Hofkens, and H. Uji-I, “Plasmon-mediated surface engineering of silver nanowires for surface-enhanced raman scattering,” *Journal of Physical Chemistry Letters*, vol. 8, no. 13, pp. 2774-2779, 2017.
- [44] R. Gupta, and W. A. Weimer, “High enhancement factor gold films for surface enhanced Raman spectroscopy,” *Chemical Physics Letters*, vol. 374, no. 3-4, pp. 302-306, 2003.